Design and verification of reduced redundancy ultrasonic MIMO arrays using simulated annealing & genetic algorithms

Sayin, Alp; Hoare, Edward; Antoniou, Michail

DOI:
10.1109/JSEN.2020.2964774

Design and Verification of Reduced Redundancy Ultrasonic MIMO Arrays using Simulated Annealing & Genetic Algorithms

Alp Sayin, Edward G. Hoare, Michail Antoniou, *Senior Member, IEEE*

***Abstract*—This paper considers methods and results on designing a reduced redundancy Multiple-Input, Multiple-Output (MIMO) ultrasonic sensor array to provide high-resolution, short-range sensing in front of a platform, while simultaneously reducing the amount of sensors required even further than a co-located MIMO array. The method proposed maximises the MIMO virtual aperture size rather than the conventional method of finding redundant physical elements to remove. This is done through adopting a Simulated Annealing and Genetic Algorithm for this problem, to optimise placement for a fixed and small number of sensor elements. The resulting array occupies less physical space than a conventional array of the same beamwidth, making it potentially attractive for small, mobile autonomous platforms. Analytical methods and simulation results are presented, and experimentally confirmed at the proof-of-concept level using a custom-built array. The experimental results verify that the proposed technique can reduce the amount of required sensor elements by 35% compared to a conventional MIMO array.**

***Index Terms*— MIMO radar, Ultrasonic Sensors, Sensor arrays.**

I. Introduction

Mobile platforms, from cars to small mobile robots, often employ ultrasonic sensors to detect obstacles and perform appropriate evasive actions [1]–[3]. This can usually be achieved by deploying a number of sensors across the body of the platform, operating independently. There is substantial research on signal processing of these individual sensors and navigation based on these independent measurements [4]–[6]. The drawback in these approaches is that angular location accuracy and angular coverage are linked to the beamwidth of each sensor; a sensor with broad beamwidth has wider coverage but lower location accuracy, while narrow beamwidth sensors yield increased accuracy but not contiguous coverage unless a larger number of sensors are used.

To solve this conflict, phased arrays can be used but this requires a relatively large number of sensors, making such a system more expensive as well as occupying a larger physical space on the platform [7]–[9]. To circumvent these limitations, a co-located MIMO sensor array is a possible solution [10]. This is because MIMO arrays have been shown to produce the same geometric pattern, with M+N transmit and receive elements, respectively, as a fully filled array with M×N transceiver modules, through appropriate spacing of the transmit and receive elements and the use of "orthogonal" transmit waveforms [11]. The MIMO array gain is less than of an equivalent phased array because there are fewer elements illuminating a target, but over relatively short ranges the sensitivity is still sufficiently high. An example of such high-resolution, short-range sensing instrument, but for radar, rather than a sonar system, and for automotive applications, can be found in [12].

The next task is to reduce the number of physical MIMO elements even further, for additional cost and physical space occupancy savings, but while simultaneously maintaining fine beamwidths. This is akin to array thinning, which is well-known for phased arrays however not so established for MIMO arrays [13]. In the latter case, work is more focused on theoretical [14]–[17] rather than experimental aspects, with a few notable exceptions [18], [19]. Additionally, the common factor in this work is that it mostly approaches array thinning by considering a fixed array aperture length and calculating the amount of physical MIMO sensor elements that can be removed while maintaining an acceptable performance. However, for short-range, high spatial resolution sensing, the number of sensors (i.e. array length) required is substantially less than what would be needed for the same spatial resolution at longer ranges, and hence the number of elements that can be redundant with such techniques is also less.

This paper explores an alternative approach; rather than fixing the array length and minimising sensor redundancy within it, it fixes the number of sensors instead, and attempts to find their locations within a longer aperture length. This improves the angular resolution of the system having the same amount of physical elements, while introducing a more substantial element reduction compared to a fully filled array of that length. Despite the reduced number of elements, an exhaustive search to find suitable element locations for acceptable performance is still computationally heavy, therefore a heuristic approach is preferred as a tool for achieving that.

Thus, the goal of the paper is to design ultrasonic MIMO array systems with a reduced redundancy compared to known co-located MIMO limits, based on the concept described above. A further reduction in the number of physical elements could

This manuscript was submitted on 28 January 2020. This project was funded by Jaguar Land Rover, UK.

M. Antoniou, E.G. Hoare are with the Department of Electronic, Electrical and Systems Engineering, University of Birmingham, Birmingham, B15 2TT UK (e-mail: m.antoniou@bham.ac.uk, e.g.hoare@bham.ac.uk).

A. Sayin was with the Department of Electronic, Electrical and Systems Engineering, University of Birmingham, Birmingham, B15 2TT UK. He is now with Novit.AI, London, EC2A 2DB UK (e-mail: alpsayin@novit.ai).

be valuable for small mobile platforms, due to the resulting savings in array physical space and required transmit power, while achieving finer beamwidths at the same time. A suitable MIMO array optimisation can be based on the well-known Simulated Annealing (SA) and Genetic Algorithm (GA), due to its established performance and relative ease of implementation [20]–[23]. To assess the validity and the performance of the approach, namely the array beamwidth, sidelobe levels, and scanning capability, a custom array was built and tested at the proof-of-concept level, while comparing experimental results to theoretical expectations.

The paper is structured as follows: Section II provides a background of generic MIMO beamforming, while Section III describes the optimisation approach followed. Section IV presents the experimental MIMO sonar array built to prove the concept, as well as the experimental process, results and their comparison with theoretical expectations.

II. Generic MIMO Array Factor

First, the conventional linear MIMO array factor is given. The array considered here comprises separate transmit (Tx) and receive (Rx) sub-arrays. For the clarification of variables and signals, a sketch of a 4x4 MIMO array is given in Fig. 1.

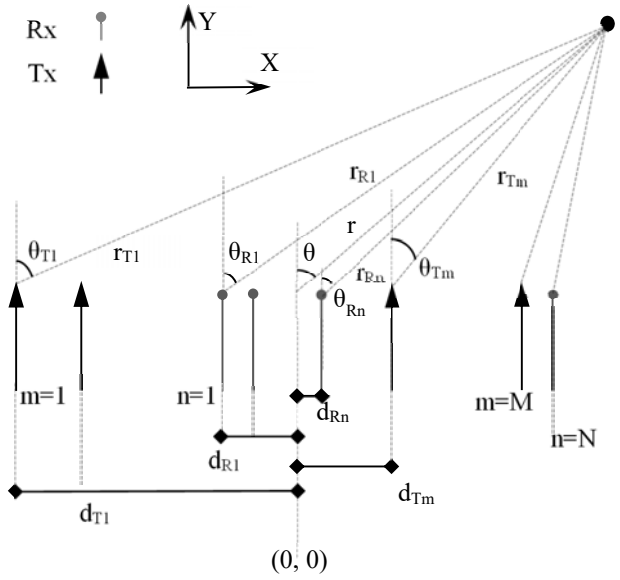

Fig. 1 MIMO array geometry

In Fig. 1 and in the following equations, θ represents the azimuth angle from the array centre to the target, where the array centre is marked as (0, 0), while θ_{Tm} and θ_{Rn} represent the individual angles from the Tx and Rx array elements, respectively. M and N represent the total number of Tx and Rx elements, respectively. Similarly, m and n are indices that are used to represent individual Tx and Rx elements. Range r represents the range from the physical centre of the array to the target, while r_{Tm} and r_{Rn} represent the individual ranges from the mth and nth Tx and Rx array elements. The variables d_{Tm} and d_{Rn} represent the individual Tx sub-array element and Rx sub-array element X-coordinates with respect to the centre of the array. It is assumed that the physical centres of the sub-arrays are at the same position and also taken as the origin of the coordinate system.

The generic MIMO array factor can be written as [10]:

$$AF_{mimo}(\theta) = \sum_{n=1}^{N} e^{-jkr_{Rn}} \sum_{m=1}^{M} e^{-jkr_{Tm}} \quad (1)$$

When the spacings d_{Rn} of the fine sub-array are equal to $\lambda/2$ and the spacings d_{Tm} of the coarse sub-array are equal to $N \times \lambda/2$, it can be shown that the resulting geometric array pattern is the same as that of a "virtual" filled phased array's with virtual elements spaced by $\lambda/2$ and a physical length of $M \times N \times \lambda/2$ also referred to as the Nyquist virtual array [24]. Such MIMO array can be steered using separate transmit and receive steering vectors, which are well-known methods (see [25], [26], for example) and are not discussed here. From Fig. 1, r_{Rn} and r_{Tm} can be written as:

$$r_{Rn} = \mathrm{r} * \cos(\theta) * \left(\left(\frac{r * sin(\theta) - d_{Rn}}{\mathrm{r} * \cos(\theta)} \right)^2 + 1 \right)^{\frac{1}{2}} \quad (2)$$

$$r_{Tm} = \mathrm{r} * \cos(\theta) * \left(\left(\frac{r * sin(\theta) - d_{Tm}}{\mathrm{r} * \cos(\theta)} \right)^2 + 1 \right)^{\frac{1}{2}} \quad (3)$$

Using (2) and (3) in (1), beamforming can be accomplished for a MIMO array. A system block diagram of this process can be seen in Fig. 2 [12]. Note that in order to perform the above operations, returns from individual Tx-Rx pairs should be accessed, and this is made possible through the use of "orthogonal" MIMO waveforms. In our case we assume this is provided through time-multiplexing transmit signals on a pulse-by-pulse basis to ensure this condition is met.

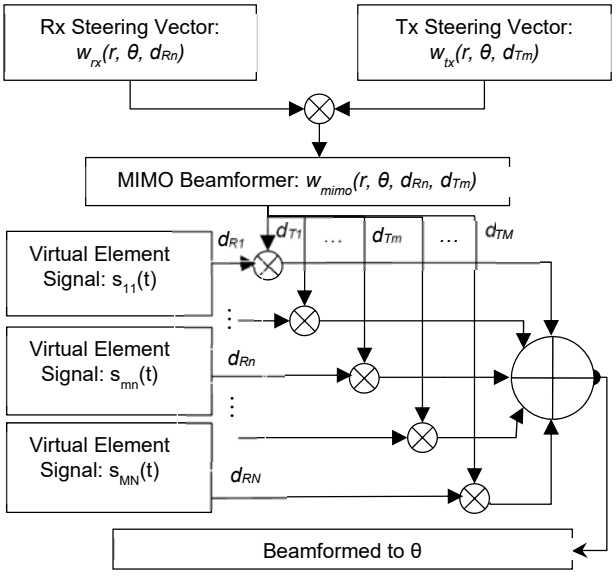

Fig. 2 Block diagram for MIMO beamformer

III. Optimisation Goals

The goal is to stretch the MIMO array by varying its element positions and testing the resulting array factor, which can still be obtained using (1), while meeting specified performance criteria. However, there is an impractically high number of

possible combinations of relative element positions to be tested, which makes the use of optimisation algorithms attractive. Once the optimal Tx and Rx positions are found for a given array length, (2) and (3) can be used to compute the array factor (1).

Two well-known algorithms, SA and GA, can be used for this task. First, SA is implemented and its outputs are then used to feed into a GA variant that is also implemented in-home and fine-tuned to generate patterns for a MIMO array for given constraints. It is common to use SA and GA in conjunction because GA's performance depends heavily on its initial population [27]. A flowchart diagram of the adopted algorithm can be seen in Fig. 3.

The general approach dictated a maximum sidelobe level and optimizing (minimising) the beamwidth (and therefore maximising the aperture size). In all iterations, some feasibility checks are undertaken to ensure that solutions are usable.

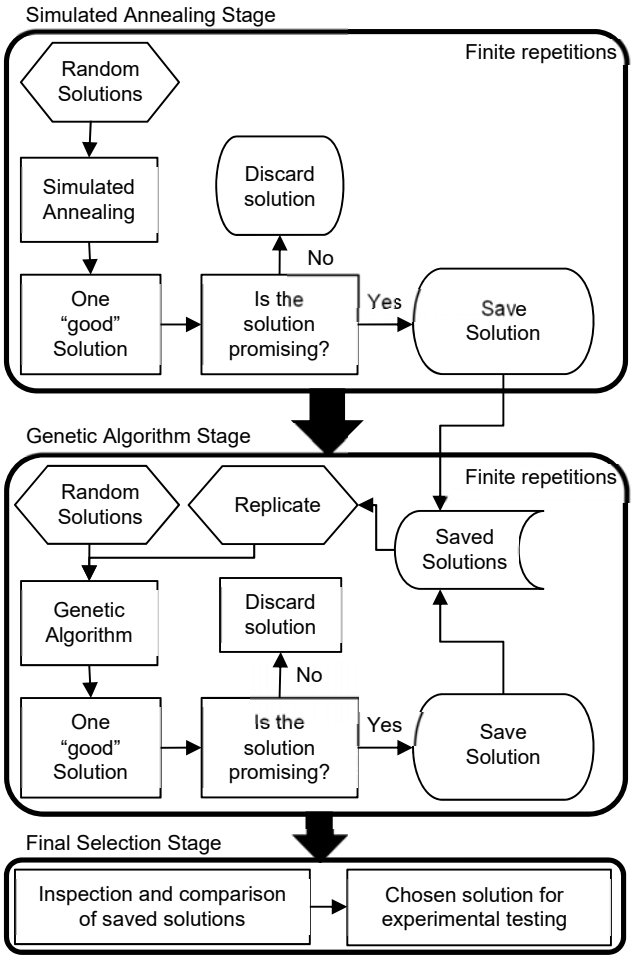

Fig. 3 Flowchart diagram of the optimisation algorithms

These feasibility checks can be summarized as;

- Absence of grating lobes
- Maximum sidelobe level requirement of -9 dB
- Having a main beam direction within 0.5 degrees
- Having acceptable edge sidelobe levels of -8 dB at maximum scan angles of -30 and 30 degrees

These checks are performed for multiple steering angles including zero, negative and positive maximum steering angles (-30 & +30 in this study). Failure in these checks adds penalties to the cost function, and therefore damages the fitness of the solution. If a solution fails in all of these checks at all of the possible scan angles, it gets the worst possible score. If a solution partially fails these checks then it rises amongst the other infeasible solutions to make path for a better neighbourhood of solutions.

Beamwidth minimization is achievable through maximizing the physical aperture. The initial solution would be the conventional MIMO array configuration. Then the algorithms test solutions of array configurations with various element positions with various array lengths. For example, if there are M transmitter and N receiver elements to be optimized, this configuration yields M-1+N variables to configure. A key constraint here is the maximum acceptable sidelobe level. Initial runs empirically showed that an acceptable sidelobe level is only achievable by imposing a limit to the maximum aperture length. Otherwise, algorithms take too long to converge, spending time dwelling on unfeasible solutions with long aperture sizes. Therefore, a maximum aperture size and a maximum acceptable sidelobe level has to be entered by the user as a parameter. Maximum physical aperture size was chosen to be 1.5 times the size of a conventional MIMO array. Also, as an optimisation constraint, a maximum tolerable sidelobe level of -9 dB has been applied. This number was chosen because a 3-4 dB increase in sidelobe levels was assumed to be tolerable for practical applications.

A. Optimisation Results

Below is an example configuration found via our algorithm. In Table I, the array configurations obtained via running the genetic algorithm can be found, along with its computed performance metrics such as sidelobe level, integrated sidelobe ratio (ISLR), mean sidelobe ratio (MSLR) and beamwidth.

TABLE I
OPTIMISED MIMO ARRAY PARAMETERS

	VALUE(S)	Unit
Transmit Antenna Positions	[0, 2.4750, 4.8044, 6.5515]	λ
Receive Antenna Positions	[0, 5.0959, 5.6294, 6.1147]	λ
Sidelobe Level	-10.5	dB
ISLR	-3.6	dB
MSLR	-13.5	dB
Beamwidth	4.3	◦

Fig. 4 shows a top view sketch of the array configuration found. On the top left the Tx array positioning and on top right the Rx array positioning can be seen separately. In addition, in the middle, the superposed transmitter and receiver configuration can be observed. Finally, at the bottom the virtual array element distribution can be observed. Those, as in the general MIMO case, can be deducted by a convolution between

the Tx and Rx element positions [10]. It should be noted that due to its asymmetrical structure, this configuration shows slight asymmetric scanning properties. However, even at relatively high steering angles all constraints are fulfilled and the simulated performance of this array scanning at 0, 30 and -30 degrees can be seen in Table II.

This configuration showed the best reduction in array elements, while still maintaining a feasible beam pattern, and thus received the highest score by the optimisation algorithm. Table III compares various metrics between the array configuration found in Table I, and conventional phased arrays as well as conventional MIMO. The table shows that the amount of elements needed for our array is approximately 3 times less than a phased array would require for the same beamwidth, at the expense of nearly 3 dB higher sidelobes. From another perspective, a conventional MIMO with the same amount of elements as our array would provide a beamwidth of 6.4 degrees, which is nearly 30% broader than that achievable by our array, but again at a penalty of 3 dB higher sidelobes.

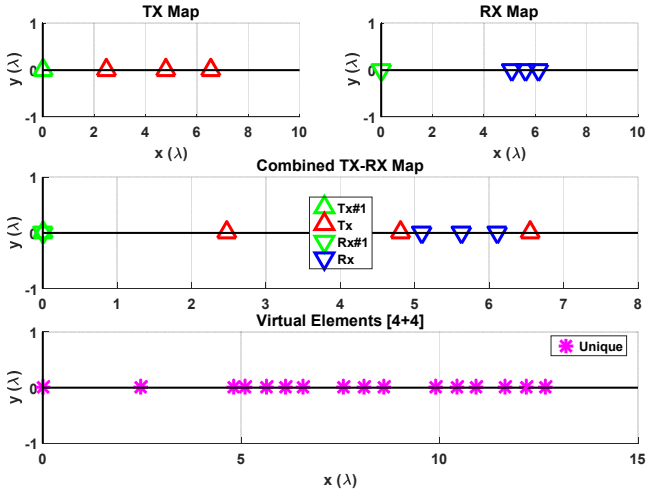

Fig. 4 Exemplary genetic algorithm optimization configuration result

TABLE II
SUMMARY OF PERFORMANCE OF OPTIMISATION RESULTS

TARGET ANGLE (DEGREES)	OPTIMISED BEAMWIDTH (DB)	PREVIOUS BEAMWIDTH (DB)	OPTIMISED SIDELOBE (DEGREES)	PREVIOUS SIDELOBE (DEGREES)
0	4.29	7.63	-10.5	-13.1
-30	4.96	8.82	-10.4	-13.1
30	4.96	8.82	-10.5	-13.1

TABLE III
COMPARISON OF PERFORMANCE WITH RESPECT TO EQUIVALENT ARRAYS

SCANNING AT 0 DEGREES	NUMBER OF ELEMENTS	BEAMWIDTH (DEGREES)	SIDELOBE (DB)
Phased Array	16	6.4	-13.1
Phased Array	24	4.2	-13.1
Conventional MIMO	8 (4x4)	6.4	-13.1
Optimised MIMO	8 (4x4)	4.2	-10.5

IV. EXPERIMENTAL RESULTS

A. *Experimental Setup*

Upon reaching a suitable element configuration, a set of trials was conducted in a quiet laboratory environment to verify the system experimentally. To this end, an ultrasonic MIMO array was built in our lab. The individual transmit and receive modules built are seen in Fig. 5, with the complete system shown in Fig.6.

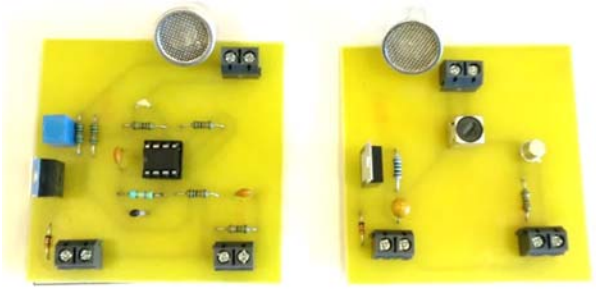

Fig. 5 Receiver (left) and transmitter (right) modules built

For the array element locations to be as precise as possible, a module housing was designed in a CAD software and 3D-printed (Fig. 7). As the diameter of the Rx sensors available was larger than the element spacings computed by the algorithm, 4 Rx elements were emulated by moving the Rx module through the 4 calculated locations, thus synthesising a 4x4 MIMO array. It is noted that as the MIMO transmission scheme was based on Time Division Multiple Access (TDMA), this arrangement does not hinder the proof-of-concept measurements.

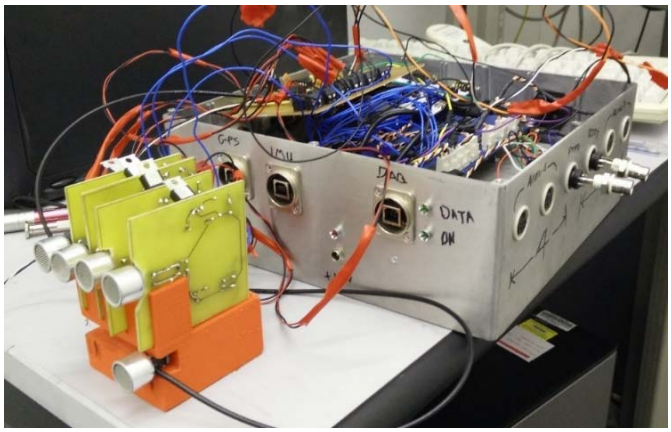

Fig. 6 Optimised MIMO sensor array housing with the sensor modules and the data acquisition box

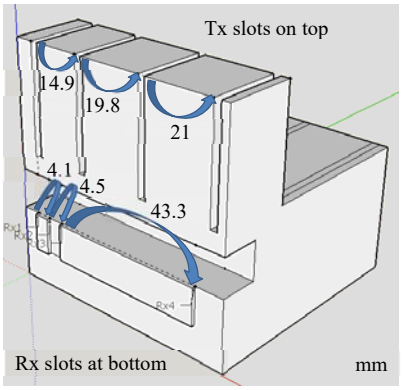

Fig. 7 3D CAD Model of sensor housing with slots and position markers. Markers are used to alternate the position of a single receive sensor

Table IV shows a summary of the parameters used in our experiments. The experimental setup error contributions were characterised and handled as follows:

1. Phase calibration of the analogue data due to acquisition equipment's characteristics,
2. reflections from other background elements (equipment itself, room door, a pedestal, corners etc.).

The most critical issue was the phase calibration, which had to be done at the signal processing level due to the acquisition board's characteristics. This was achieved by using a reference target at a known location and phase calibrating the virtual element signals. Knowing the position of the reference target, the expected dominant signal phases at a specific range were computed and compensated. For the sake of simplicity, reference targets have been cropped out from the results.

TABLE IV
EXPERIMENT PARAMETERS

EXPERIMENT PROPERTY	VALUE	UNIT
Number of Tx	4	-
Number of Rx	4	-
Multiple Access Scheme	TDMA	-
Carrier Frequency	40	kHz
Wavelength	8.38	mm
Waveform	Up-chirp LFM	-
Bandwidth	4	kHz
Tx Sensor Beamwidth	55	Degrees
Rx Sensor Beamwidth	55	Degrees
Receive Gain	~20	dB
Tx Element Positions	[0, 20.73, 40.24, 54.87]	mm
Rx Element Positions	[0, 42.68, 47.15, 51.21]	mm
Sample Rate	250,000	Samples/s
Pulse length	0.08	Seconds
PRI	0.25	Seconds

B. *Scenarios and Results*

Experiments were performed using a target placed at ranges varying from 1.7m to 2.2m from the sonar and changing azimuth angles. Target measurements were made at 0, 15, 20 and 25 degrees to test the angular width over which beamforming can operate. These scenarios were designed to check beamforming and target locating capabilities, as well as azimuth resolution. The physical setup inside the test chamber with one of the experimental scenarios is shown in Fig. 8.

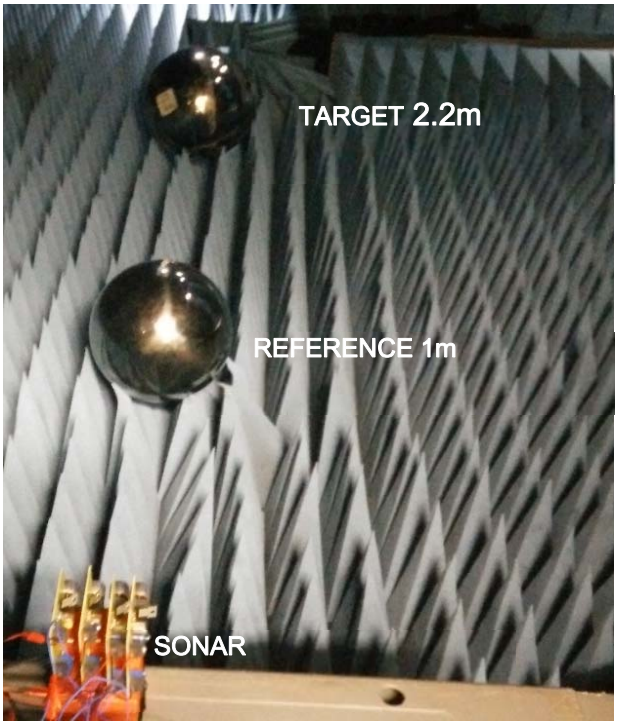

Fig. 8 Photo of the experimental setup where target is at 0 degrees

Experiments were undertaken with calibrated targets as before to verify the computed parameters such as beamwidth and sidelobe levels. Throughout the following figures range-azimuth maps obtained from measurements without any post-processing method but with the omission of the phase calibration reference can be seen. Along with them are the azimuth cuts at the corresponding target ranges in which the target responses are compared to our simulated results. In all of the measurement scenarios we can see a strong reflection at the expected location coinciding with target's physical position and we also observe a strong correlation of experimental and simulated results in azimuth cuts.

1) Target at 0 Degrees

In Fig. 9 the range-azimuth map and in Fig. 10 the azimuth cut from target at 0-degree scenario can be seen.

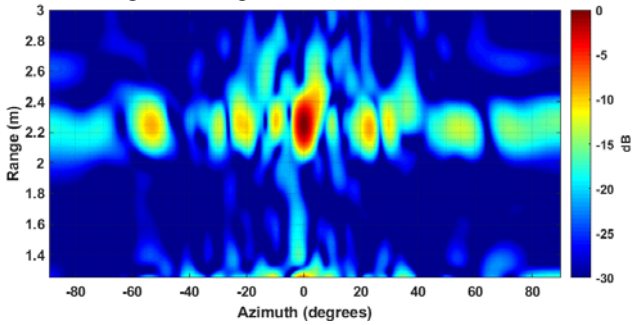

Fig. 9 Target at 0 degrees; range-angle map

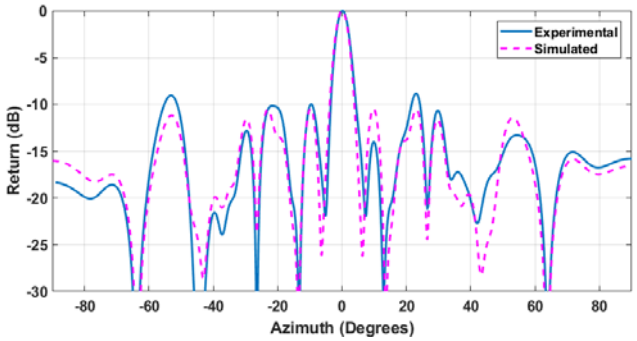

Fig. 10 Target at 0 degrees; azimuth cut at target range

2) Target at 15 Degrees

In Fig. 11 the range-azimuth map and in Fig. 12 the azimuth cut from target at 15-degree scenario can be seen.

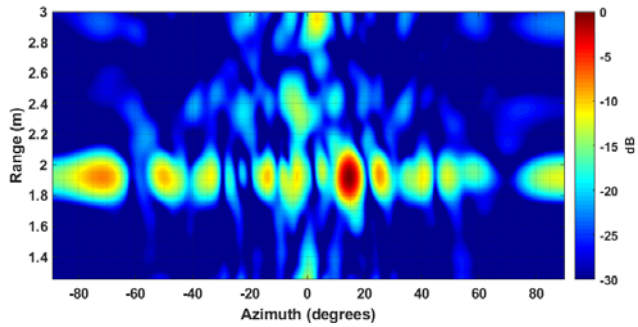

Fig. 11 Target at 15 degrees; range-angle map

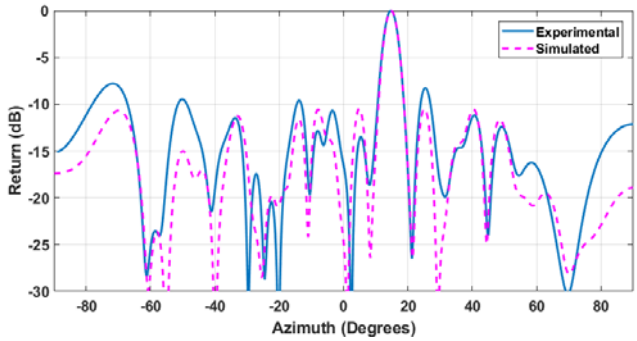

Fig. 12 Target at 15 degrees; range-angle map

3) Target at 20 Degrees

In Fig. 13 the range-azimuth map and in Fig. 14 the azimuth cut from target at 20-degree scenario can be seen.

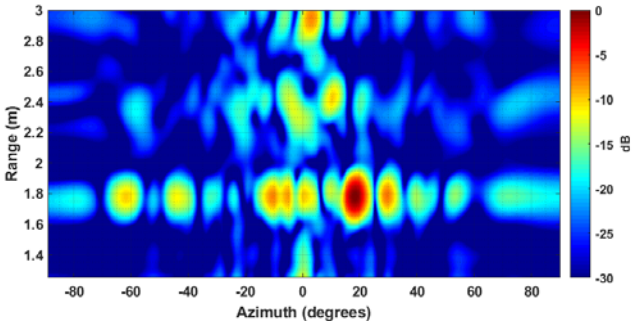

Fig. 13 Target at 20 degrees; range-angle map

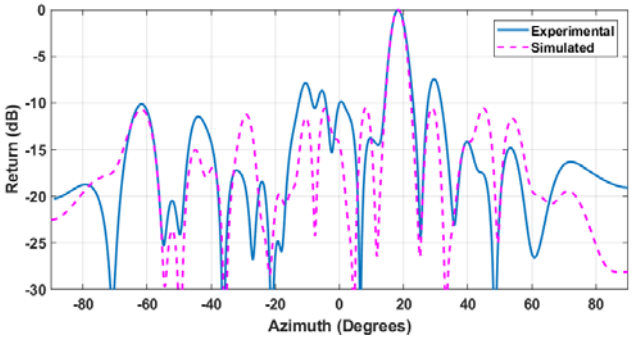

Fig. 14 Target at 20 degrees; azimuth cut at target range

4) Target at 25 Degrees

In Fig. 15 the range-azimuth map and in Fig. 16 the azimuth cut from target at 25-degree scenario can be seen.

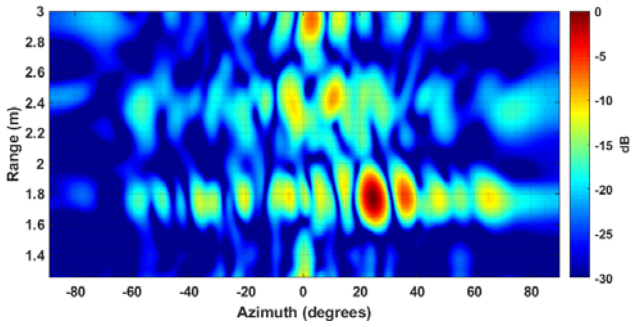

Fig. 15 Target at 25 degrees; range-angle map

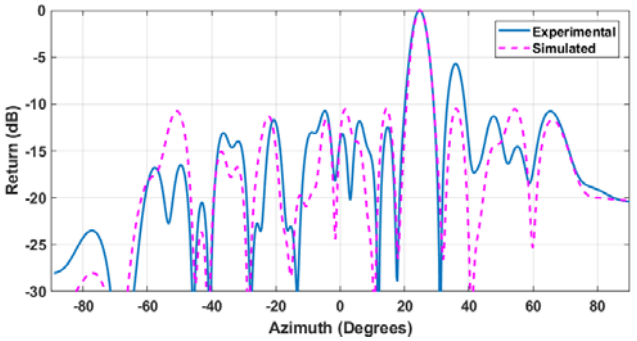

Fig. 16 Target at 25 degrees; azimuth cut at target range

Finally, a summary of performance measurements from all experiments can be seen in below; Table V with sidelobe and beamwidth measurements and Table VI with integrated and mean sidelobe ratios.

TABLE V
SUMMARY OF SIDELOBE PERFORMANCE OF EXPERIMENTAL RESULTS

TARGET ANGLE (DEGREES)	EXPERIMENT SIDELOBE (DB)	SIMULATION SIDELOBE (DB)	EXPERIMENT BEAMWIDTH (DEGREES)	SIMULATION BEAMWIDTH (DEGREES)
0	-8.8	-10.5	4.31	4.29
15	-7.8	-10.5	4.54	4.45
20	-7.4	-10.5	4.79	4.57
25	-5.7	-10.5	4.93	4.74

TABLE VI
SUMMARY OF ISLR AND MSLR PERFORMANCE OF EXPERIMENTAL RESULTS

TARGET ANGLE (DEGREES)	EXPERIMENT ISLR (DB)	SIMULATION ISLR (DB)	EXPERIMENT MSLL (DB)	SIMULATION MSLL (DB)
0	-3.6	-3.6	-13.4	-13.5
15	-3.2	-3.8	-12.9	-13.8
20	-3.9	-4.0	-13.6	-13.8
25	-4.0	-4.3	-14.0	-14.0

Overall, the experiments yielded results which matched simulations. In summary, the optimised MIMO configuration tested has about 4.25 degrees beamwidth with only 8 elements, with around -8.8 dB sidelobe levels (scanning to broadside). This is equivalent to 35% improvement with respect to a conventional 8 element MIMO array or a 16-element phased array. Or in other words it has the equivalent beamwidth of a 24-element phased array.

V. CONCLUSIONS AND FUTURE WORK

The design of ultrasonic MIMO arrays with a reduced redundancy has been considered. The approach to optimise the number of physical elements was based on SA&GA. Following this approach, a 4x4 MIMO array was designed, which can achieve a 4.2-degree beamwidth and a field of view of 50 degrees. The resulting beamwidth is the equivalent of a 24-element phased array, whereas a conventional co-located 4x4 MIMO array would be the equivalent of a 16-element phased array. Through the development of an experimental system and its testing, the feasibility and performance of the array was confirmed, with comparable simulation results. The next step in this research is to consider alternative optimisation methods, and experimentally compare their relative merits and drawbacks to what has been developed here.

REFERENCES

[1] C. De Marziani *et al.*, "Simultaneous Round-Trip Time-of-Flight Measurements With Encoded Acoustic Signals," *IEEE Sensors Journal*, vol. 12, no. 10, pp. 2931–2940, Oct. 2012.

[2] D. Ratner and P. McKerrow, "Navigating an outdoor robot along continuous landmarks with ultrasonic sensing," *Robotics and Autonomous Systems*, vol. 45, no. 2, pp. 73–82, Nov. 2003.

[3] K.-W. Jorg and M. Berg, "Mobile robot sonar sensing with pseudo-random codes," 1998, vol. 4, pp. 2807–2812.

[4] J. Steckel and H. Peremans, "A novel biomimetic sonarhead using beamforming technology to mimic bat echolocation," *IEEE Transactions on Ultrasonics, Ferroelectrics, and Frequency Control*, vol. 59, no. 7, pp. 1369–1377, Jul. 2012.

[5] D. Bank and T. Kampke, "High-Resolution Ultrasonic Environment Imaging," *IEEE Transactions on Robotics*, vol. 23, no. 2, pp. 370–381, Apr. 2007.

[6] B. Barshan and R. Kuc, "A bat-like sonar system for obstacle localization," *IEEE Transactions on Systems, Man, and Cybernetics*, vol. 22, no. 4, pp. 636–646, Aug. 1992.

[7] C. Diego, A. Jimenez, A. Hernandez, C. J. Martin-Arguedas, and C. G. Fernandez, "Improved Ultrasonic Phased Array Based on Encoded Transmissions for Obstacle Detection," *IEEE Sensors Journal*, vol. 15, no. 2, pp. 827–835, Feb. 2015.

[8] Hongbo Zhu, H. Inubushi, N. Takahashi, and K. Taniguchi, "An ultrasonic 3D image sensor employing PN code," 2006, pp. 319–322.

[9] P. Webb and C. Wykes, "High-resolution beam forming for ultrasonic arrays," *IEEE Transactions on Robotics and Automation*, vol. 12, no. 1, pp. 138–146, Feb. 1996.

[10] M. A. Richards, J. A. Scheer, and W. A. Holm, *Principles of modern radar. vol. 2, vol. 2,*. Raleigh, N.C.: SciTech Pub., 2010.

[11] D. W. Bliss and K. W. Forsythe, "Multiple-input multiple-output (MIMO) radar and imaging: degrees of freedom and resolution," in *Signals, Systems and Computers, 2003. Conference Record of the Thirty-Seventh Asilomar Conference on*, 2003, vol. 1, pp. 54–59.

[12] A. Sayin, S. Pooni, E. Hoare, and M. Antoniou, "MIMO array for short-range, high-resolution automotive sensing," *IET Radar, Sonar Navigation*, vol. 12, no. 10, pp. 1165–1171, 2018.

[13] R. C. Hansen, *Phased array antennas*, 2nd ed. Hoboken, N.J: Wiley, 2009.

[14] X. Liu, C. Sun, Y. Yang, J. Zhuo, and Y. Han, "Low complexity MIMO sonar imaging using a virtual sparse linear array," *Journal of Systems Engineering and Electronics*, vol. 27, no. 2, pp. 370–378, Apr. 2016.

[15] A. Kirschner, U. Siart, J. Guetlein, and J. Detlefsen, "A design-algorithm for MIMO radar antenna setups with minimum redundancy," in *Microwaves, Communications, Antennas and Electronics Systems (COMCAS), 2013 IEEE International Conference on*, 2013, pp. 1–5.

[16] J. Dong, R. Shi, Y. Guo, and W. Lei, "Antenna array design in MIMO radar using cyclic difference sets and genetic algorithm," in *Antennas, Propagation & EM Theory (ISAPE), 2012 10th International Symposium on*, 2012, pp. 26–29.

[17] P. F. Sammartino, D. Tarchi, and C. J. Baker, "MIMO radar topology: A systematic approach to the placement of the antennas," in *Electromagnetics in Advanced Applications (ICEAA), 2011 International Conference on*, 2011, pp. 114–117.

[18] C. Vasanelli, R. Batra, and C. Waldschmidt, "Optimization of a MIMO radar antenna system for automotive applications," in *2017 11th European Conference on Antennas and Propagation (EUCAP)*, Paris, France, 2017, pp. 1113–1117.

[19] K. Rezer, C. Klickow, and A. F. Jacob, "Thinned MIMO frame-arrays for radar imaging," in *Microwave Symposium Digest (MTT), 2012 IEEE MTT-S International*, 2012, pp. 1–3.

[20] S. Kirkpatrick, M. P. Vecchi, and others, "Optimization by simmulated annealing," S*cience*, vol. 220, no. 4598, pp. 671–680, 1983.

[21] V. Černỳ, "Thermodynamical approach to the traveling salesman problem: An efficient simulation algorithm," *Journal of optimization theory and applications*, vol. 45, no. 1, pp. 41–51, 1985.

[22] J. H. Holland, *Adaptation in natural and artificial systems: an introductory analysis with applications to biology, control, and artificial intelligence*, 1st MIT Press ed. Cambridge, Mass: MIT Press, 1992.

[23] C. R. Reeves and J. E. Rowe, *Genetic algorithms: principles and perspectives: a guide to GA theory*. Boston: Kluwer Academic Publishers, 2003.

[24] K. W. Forsythe and D. W. Bliss, "MIMO Radar Waveform Constraints for GMTI," *IEEE Journal of Selected Topics in Signal Processing*, vol. 4, no. 1, pp. 21–32, Feb. 2010.

[25] M. A. Richards, J. Scheer, W. A. Holm, and W. L. Melvin, Eds., *Principles of modern radar*. Raleigh, NC: SciTech Pub, 2010.

[26] J. Li and P. Stoica, Eds., *MIMO radar signal processing*. Hoboken, NJ: J. Wiley & Sons, 2009.

[27] M. Andresen, H. Bräsel, M. Mörig, J. Tusch, F. Werner, and P. Willenius, "Simulated annealing and genetic algorithms for minimizing mean flow time in an open shop," *Mathematical and Computer Modelling*, vol. 48, no. 7–8, pp. 1279–1293, Oct. 2008.